

# Enhanced Raman Scattering of CuPc Films on Imperfect WSe<sub>2</sub> Monolayer Correlated to Exciton and Charge-Transfer Resonances

Yanran Liu, Zhibin Gao, Ming Chen, Yang Tan,\* and Feng Chen\*

Recently, 2D transition-metal dichalcogenides (2D TMDCs) are identified as ideal substrates for surface-enhanced Raman scattering (SERS). However, the effect of enhancement factor (EF) on TMDCs is lower than metal-based SERS substrates. Here, it is demonstrated that the SERS performance of WSe<sub>2</sub> monolayer can be enhanced via tailoring the atomic ratio of WSe<sub>2</sub>; this correlates to the exciton and charge-transfer resonances. CuPc molecules are adsorbed onto WSe<sub>2</sub> monolayers as the probe molecules, and the atomic ratio (Se:W) of WSe<sub>2</sub> is tailored from 2 to 1.92. For an atomic ratio of 1.96, the maximum EF on irradiated WSe<sub>2</sub> is more than 120; this is enhanced by more than 40 times compared with pristine WSe<sub>2</sub>. The amplitude of exciton and charge-transfer resonances is estimated by femtosecond optical pump-probe measurement and a bipolar junction transistor (BJT) consisting of CuPc film and 2D materials. It is found that the intensity of resonances in the CuPc–WSe<sub>2</sub> system is tailored by the atomic ratio of WSe<sub>2</sub>. This is closely correlated to the SERS performance of WSe<sub>2</sub>. This study shows that the SERS performance of WSe<sub>2</sub> is enhanced by tuning the atomic ratio of WSe<sub>2</sub> and provides qualitative theoretical explanations for the mechanism of enhanced SERS.

## 1. Introduction

Surface-enhanced Raman spectroscopy (SERS) is one of the most sensitive techniques for the detection of surface species. SERS allows ultrasensitive detection down to a single molecule and provides information about the structure of molecules via their unique Raman spectra.<sup>[1–3]</sup> In the SERS measurements, the material of SERS substrate plays an important role, as

significant enhancement of Raman signals can be obtained from the substrate via two mechanisms, i.e., electromagnetic mechanism (EM) and chemical mechanism (CM). EM involves the enhancement of local electromagnetic field intrigued by surface plasmons excited by the incident light;<sup>[4,5]</sup> CM involves the vibronic coupling of exciton and charge-transfer (CT) resonances induced by photonic excitation.<sup>[6–9]</sup> Noble metals such as Au, Ag, and Cu are traditional SERS substrates owing to the existence of EM. However, noble metals have several disadvantages as SERS substrates, including high cost, poor uniformity, and lack of stability, thus limiting the applications of noble-metal SERS substrates.<sup>[10–12]</sup> In contrast to noble metals, semiconductor SERS substrates have gained immense popularity;<sup>[13–15]</sup> they not only have higher SERS uniformity, but also better chemical stability and low cost.<sup>[16,17]</sup> The mechanism of


semiconductor SERS substrates involves CM that is correlated to the vibronic coupling of exciton and charge-transfer resonances in a molecule–semiconductor system.<sup>[7–9]</sup> Nevertheless, the detailed mechanism of these resonances in SERS remains poorly understood.

Recently, 2D transition-metal dichalcogenides (2D TMDCs), semiconducting materials, have been studied as possible candidates for SERS substrates.<sup>[18–20]</sup> 2D TMDCs are usually denoted as MX<sub>2</sub>, where M and X represent transition metals such as Mo, W, and Ta and chalcogens (S, Se, and Te), respectively.<sup>[21]</sup> TMDCs have been shown to be effective SERS substrates with many advantages.<sup>[22]</sup> For example, TMDCs are much easier to combine with traditional noble metals, allowing to take the advantage of both metals and semiconductor substrates. In addition, TMDCs are flexible substrates, beneficial for the detection of food additives. The main SERS mechanism of TMDCs involves CM, providing an ideal environment for extensive study of CM. However, the enhancement factor (EF) of a pristine TMDCs substrate ( $\approx 10$ ) is generally much lower than a noble-metal substrate ( $10^6$ – $10^{10}$ ),<sup>[23]</sup> far from the requirement of chemical and biological sensing. Therefore, it is necessary to explore novel strategies to improve the SERS performance of TMDCs.<sup>[14,24–27]</sup>

Fortunately, the enthusiastic attention of 2D TMDCs is not limited to intrinsic material properties, but also their adjustable

Y. Liu, Dr. M. Chen, Prof. Y. Tan, Prof. F. Chen  
School of Physics  
State Key Laboratory of Crystal Materials  
Shandong University  
Jinan 250100, China  
E-mail: tanyang@sdu.edu.cn; drfchen@sdu.edu.cn

Dr. Z. Gao  
Center for Phononics and Thermal Energy Science  
China-EU Joint Center for Nanophononics  
Shanghai Key Laboratory of Special Artificial Microstructure  
Materials and Technology  
School of Physics Sciences and Engineering  
Tongji University  
Shanghai 200092, China

 The ORCID identification number(s) for the author(s) of this article can be found under <https://doi.org/10.1002/adfm.201805710>.

DOI: 10.1002/adfm.201805710

features.<sup>[28,29]</sup> The electronic structure of TMDCs can be efficiently tuned by adjusting the chemical composition or atomic arrangement of TMDCs. For example, the electronic states and bandgap of 2D TMDC semiconductors could be tuned by using defects<sup>[30,31]</sup> or chemical doping.<sup>[28]</sup> As a great platform, 2D TMDCs allow the adjustment of material properties to achieve the desired function, providing opportunities for wide applications. Ion irradiation is a well-known method for the modification of 2D materials.<sup>[32,33]</sup> Through the collision with incident energetic ions, the atoms in a material can be sputtered or displaced, thus tailoring the atomic ratio of material and leading to the variation of electronic structure and material properties. Therefore, it is a potential strategy to tailor the atomic ratio of TMDCs by ion irradiation to improve the SERS performance of TMDCs.

In this study, we demonstrate that the SERS performance of WSe<sub>2</sub> monolayer can be enhanced by tuning the atomic ratio. To demonstrate the magnification mechanism of observed SERS, we carried out the quantitative detection of charge-transfer and exciton resonances in the molecule–WSe<sub>2</sub> system via fs optical pump-probe measurement<sup>[34,35]</sup> and a bipolar junction transistor (BJT).<sup>[36,37]</sup> It was found that the EF is enhanced by more than 40 times on WSe<sub>2</sub> monolayer with an atomic ratio of 1.96 compared with the pristine WSe<sub>2</sub> monolayer. At the same atomic ratio, the quantity of exciton increased by nine times, and the charge-transfer current between the probe molecule and WSe<sub>2</sub> increased by 9.4 times. This is correlated to the enhancement of SERS. This study demonstrates that the tuning of atomic ratio is a novel methodology to engineer the electronic structure of TMDCs and helps to achieve better applications of TMDCs for SERS.

## 2. Results and Discussion

### 2.1. Tailored Atomic Ratio of WSe<sub>2</sub> Monolayers

The WSe<sub>2</sub> monolayer was fabricated by chemical vapor deposition (CVD) method and transferred onto a Cu wire mesh. The structure of as-prepared suspended WSe<sub>2</sub> (*S*<sub>0</sub>) was detected by transmission electron microscopy (TEM) as shown in Figure 1a, exhibiting the periodic atomic arrangement of WSe<sub>2</sub> monolayer and demonstrating a high crystalline nature of the as-prepared WSe<sub>2</sub>. The thickness of WSe<sub>2</sub> is ≈0.8 nm, as measured by atomic force microscopy (AFM) as shown in Figure 1b, corresponding to a monolayer thickness. The elemental analysis of as-prepared WSe<sub>2</sub> monolayer was performed by energy-dispersive X-ray spectroscopy (EDX) as shown in Figure 1c, indicating that the as-prepared WSe<sub>2</sub> has a stoichiometric ratio of Se:W ≈ 2.

To artificially tailor the atomic ratio (Se:W) of suspended WSe<sub>2</sub> monolayer, we irradiated the as-prepared WSe<sub>2</sub> monolayers by Au ion beam with an energy of 500 keV and controlled dose/fluence (*S*<sub>1</sub> = 1 × 10<sup>12</sup> ions cm<sup>-2</sup>; *S*<sub>2</sub> = 1 × 10<sup>13</sup> ions cm<sup>-2</sup>; and *S*<sub>3</sub> = 1 × 10<sup>14</sup> ions cm<sup>-2</sup>). During the ion irradiation, the energetic Au ion impacted and penetrated the WSe<sub>2</sub> monolayer (Part I, Supporting Information)<sup>[28,29]</sup> (Figure 1d). The evolution of atomic ratio of irradiated WSe<sub>2</sub> was detected by X-ray photoelectron spectroscopy (XPS). Figure 1e shows the high-resolution XPS spectra of W-4f and Se-3d for *S*<sub>0</sub> and *S*<sub>3</sub>, respectively. The intensity of Se-3d peaks decreased after the irradiation, while the intensity of W-4f remained unchanged. This indicates that Se atoms were bombed away from the top

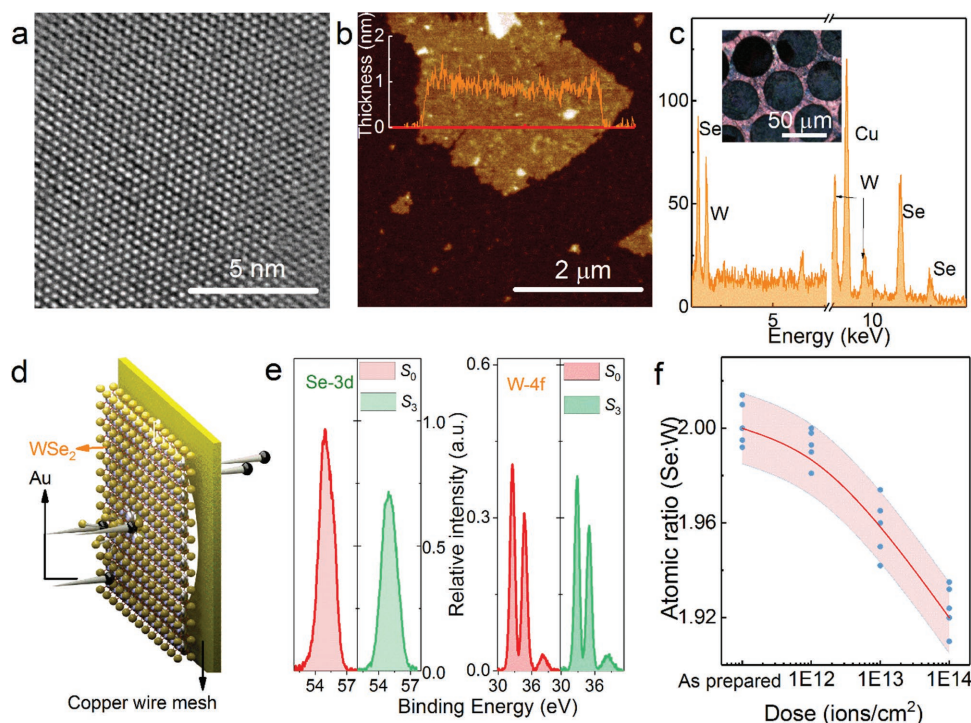


**Figure 1.** a) TEM, b) AFM, and c) EDX images of as-prepared WSe<sub>2</sub> monolayer. The inset in (c) shows the photograph of WSe<sub>2</sub> monolayer suspended on a Cu wire mesh. d) Schematic diagram of Au ion irradiation. e) XPS image of irradiated WSe<sub>2</sub> monolayer with a fluence of 1 × 10<sup>14</sup> ions cm<sup>-2</sup> (*S*<sub>3</sub>). f) Evolution of atomic ratio with the fluence of incident ions.

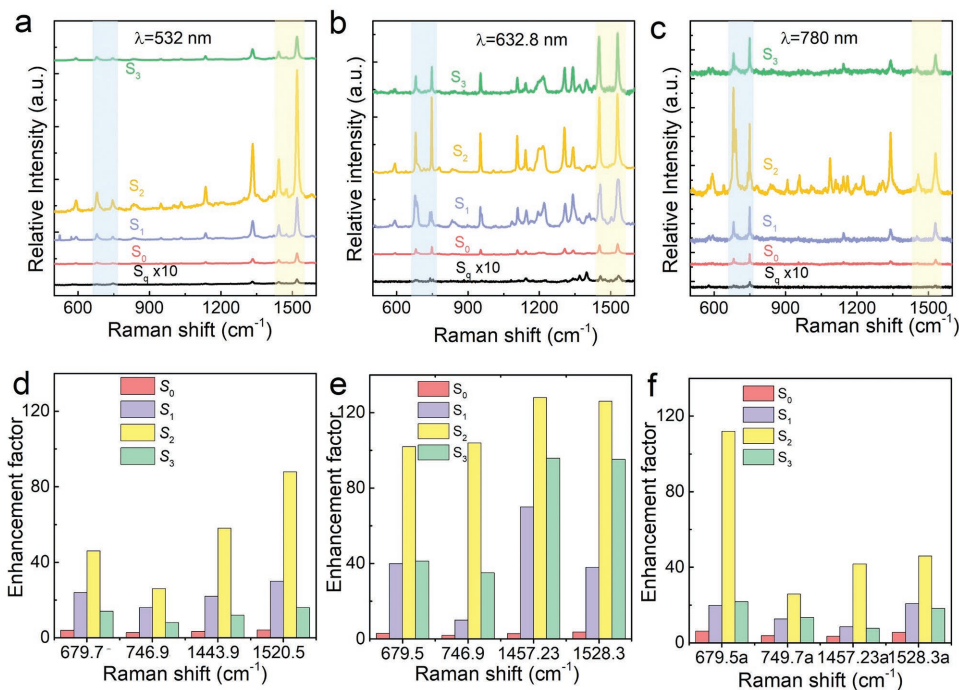


**Figure 2.** Measured Raman spectroscopy of as-prepared ( $S_0$ ) and irradiated  $\text{WSe}_2$  monolayers ( $S_1$ ,  $S_2$ , and  $S_3$ ), excited by a laser at a) 532 nm, b) 632.8 nm, and c) 780 nm. EFs corresponding to the illumination laser at d) 532 nm, e) 632.8 nm, and f) 780 nm.

atomic layer of  $\text{WSe}_2$ , leaving Se-vacancies. With the increase in dose, the Se:W atomic ratio gradually decreased from 2 to 1.92. This indicates that the density of Se-vacancy can be controlled by the dosage of incident ion beams (Figure 1f).

## 2.2. SERS Properties of $\text{WSe}_2$ Monolayers with Tailored Atomic Ratio

Interestingly, different SERS behaviors were observed on the as-prepared and irradiated  $\text{WSe}_2$  monolayers, as shown in Figure 2. The SERS properties of these samples ( $S_0$ ,  $S_1$ ,  $S_2$ , and  $S_3$ ) were detected using Cu phthalocyanine (CuPc) molecules as the target molecules; CuPc was coated onto samples using the Langmuir–Blodgett (LB) technique. Figure 2a–c shows the Raman spectra of CuPc film (thickness of  $\approx 1$  nm) with the excitation laser at a wavelength ( $\lambda_e$ ) of 532, 632.8, and 780 nm, respectively. The laser power of excitation laser is 1 mW, and the exposure time is 60 s. One key observation is that the energy distribution between vibrational modes in SERS spectra depends on the wavelength of excitation laser. For example, the Raman signals at high-frequency modes (1443.9, 1520.5  $\text{cm}^{-1}$ ) are excited by a 532 nm laser; however, both high frequency ( $\approx 1457$   $\text{cm}^{-1}$ ,  $\approx 1528$   $\text{cm}^{-1}$ ) and low frequency ( $\approx 680$   $\text{cm}^{-1}$ ,  $\approx 747$   $\text{cm}^{-1}$ ) vibrational modes are excited by 632.8-nm (1457.2, 1528.3, 748, and 679.5  $\text{cm}^{-1}$ ) and 780 nm (1457.8, 1530, 749.2, and 680.7  $\text{cm}^{-1}$ ) lasers.

Another observation is that the irradiated  $\text{WSe}_2$  ( $S_1$ ,  $S_2$ , and  $S_3$ ) produces stronger SERS signals of CuPc molecules than those on the as-prepared  $\text{WSe}_2$  ( $S_0$ ). To quantitatively compare the SERS activities of samples, we calculated the EF per molecule based on the magnification of Raman

intensity compared with that on a bare quartz wafer (labeled as  $S_q$ ) (Part II, Supporting Information). Here, the vibrational modes at  $\approx 1520$   $\text{cm}^{-1}$  were analyzed and accurately assigned in the SERS spectra excited by all the light. When excited by a 532 nm laser, the EFs were 4.1, 30.2, 88.4, and 16.6, corresponding to the platforms of  $S_0$ ,  $S_1$ ,  $S_2$ , and  $S_3$ , where  $S_2$  with a Se:W ratio ( $R$ ) of 1.96 has the highest EF (Figure 2d). A similar phenomenon was also observed with the 632.8 nm and 780 nm excitation lasers. For 632.8 nm (780 nm) laser,  $S_2$  has the highest EF with a value of 126 (45.8), and the value of EF decreased to 95.2 (18.2) on  $S_3$  (Figure 2e,f). Notably, with the excitation of 632.8 nm laser, the EF on  $S_2$  was over 120 at the vibrational modes of 1457.2 and 1528.3  $\text{cm}^{-1}$ , more than 40 times higher than that on  $S_0$  (1457.2  $\text{cm}^{-1}$ : EF = 3; 1528.3  $\text{cm}^{-1}$ : EF = 3.4).

## 2.3. Mechanism of SERS Enhancement Induced by Irradiation

Our experiments show that an EF of over 120 can be achieved on irradiated  $\text{WSe}_2$  monolayer with a specific atomic ratio (or density of defects). This value is much higher than that previously observed on graphene and all other pristine 2D materials.<sup>[18–20,37]</sup> On pristine  $\text{WSe}_2$ , the SERS can be explained by semiconductor mechanism, where the vibronic coupling of exciton and charge-transfer resonances is considered. For the exciton transition, a vibrational quantum of energy is transferred to the vibrational level of CuPc molecule, thus inducing the radiation of a Raman photon from the CuPc molecule to the vibrational states. For the charge-transfer resonance, the photon-induced charges are transferred from the band edges of  $\text{WSe}_2$  to the affinity levels of CuPc molecules. This changes

the polarizability of molecule, leading to the magnification of Raman signals. To elucidate the magnification mechanism of observed SERS, we need the quantitative detection of these two resonances. In the following sections, the variation in resonances was experimentally measured.

### 2.3.1. Exciton Resonance

Excitons are optically excited electron–hole pairs in WSe<sub>2</sub>. The dynamic nature of excitons in the illuminated WSe<sub>2</sub> can be detected by fs optical pump-probe spectroscopy. During the fs pump-probe measurement, the excitons present in the WSe<sub>2</sub> monolayer are excited using a pump light (a 400 nm and 100 fs laser pulse with a peak fluence of 200 μJ cm<sup>-2</sup>), inducing photobleaching ( $\Delta T > 0$ ) due to screen effects. Moreover, a probe light with a wide broadband (440–740 nm) was used to detect the time-resolved different transmission ( $\Delta T/T_0$ ) of WSe<sub>2</sub>. In the transmission spectra, the reduced absorption of  $\Delta T/T_0$  is directly proportional to the quantity of excitons (Part III, Supporting Information). **Figure 3a–c** shows the measured transmission spectra of as-prepared and irradiated WSe<sub>2</sub> monolayers (*S*<sub>0</sub>, *S*<sub>2</sub>, and *S*<sub>3</sub>). In all the samples, the exciton resonances are localized at a wavelength of 510, 596, and 744 nm, corresponding to the resonances at A', B, and A. When the atomic ratio was decreased to 1.96 (*S*<sub>2</sub>), the quantity of exciton was almost nine times compared with the as-prepared one (Figure 3d). When the ratio was continuously decreased to *S*<sub>3</sub> (1.92), the quantity was lower than *S*<sub>2</sub>, but larger than *S*<sub>0</sub> at all the exciton resonances. Two astonishing features of WSe<sub>2</sub> could be deduced. 1) The quantity of exciton can be adjusted by tuning the atomic ratio of WSe<sub>2</sub> monolayer. 2) The shape and peak position of exciton resonances are similar for different atomic ratios.

To further establish the relationship between atomic ratio and exciton, the evolution of electronic structure of WSe<sub>2</sub> was

calculated according to the first-principle method. Using the plane wave basis Vienna ab initio simulation package, the total density of states (TDOS) of WSe<sub>2</sub> monolayers with atomic ratios (Se:W) of 2, 1.96, and 1.91666 are shown in Figure 3e (Part IV, Supporting Information). With the atomic ratio of 1.96, there is an obvious increase in TDOS compared with the pristine one, and an extra intermediate state emerged between the valence and conduction bands. When the ratio was decreased to 1.91666, the TDOS at the intermediate state increased, whereas the average TDOS slightly decreased compared to that with 1.96. These calculated results show that the TDOS of WSe<sub>2</sub> monolayer can be artificially tailored by adjusting the atomic ratio. Furthermore, the evolution of TDOS is similar to the change in excitons observed in Figure 3d. It seems that there is a relationship between the variation in exciton and TDOS adjusted using the atomic ratio. The physical reason of the difference between *S*<sub>2</sub> and *S*<sub>3</sub> is that more Se vacancies will decrease the supply of number of electrons to the whole WSe<sub>2</sub> system. The midgap states in TDOS of *S*<sub>3</sub> is smaller than *S*<sub>2</sub>, indicating less electrons provision. As we known, excitons are describing electron-hole pairs. Hence, the optical absorption of *S*<sub>3</sub> is smaller than *S*<sub>2</sub> but still quite large than *S*<sub>0</sub> situation.<sup>[36]</sup>

### 2.3.2. Charge-Transfer Resonance

To identify the charge-transfer transitions in the CuPc deposited WSe<sub>2</sub> film, we measured the UV–vis absorption spectra of CuPc molecules deposited on WSe<sub>2</sub> subtracting the absorption spectra of neat CuPc molecules and the WSe<sub>2</sub> monolayer. **Figure 4** shows observed CT absorption for as-prepared (*S*<sub>0</sub>) and irradiated WSe<sub>2</sub> monolayers (*S*<sub>2</sub>, *S*<sub>3</sub>). The results originated from different samples illustrate that the CT absorption peaks in visible region are observed at same positions, while the relative intensities are slightly enhanced by changing the target from *S*<sub>0</sub> to *S*<sub>2</sub> and then *S*<sub>3</sub>. For example, the maximum

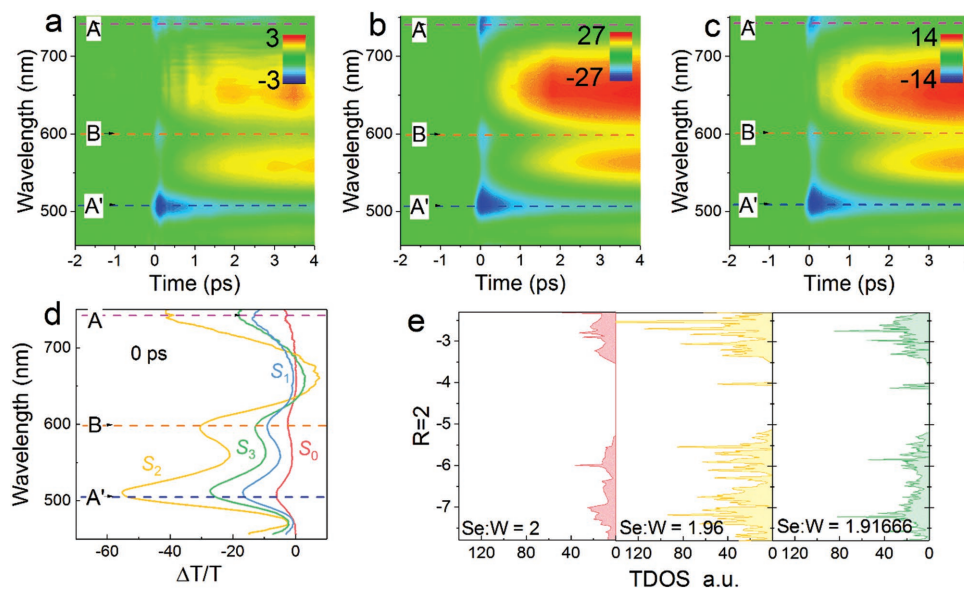


**Figure 3.** fs optical pump-probe spectroscopy ( $\Delta T/T_0$ ) of a) *S*<sub>0</sub>, b) *S*<sub>2</sub>, and c) *S*<sub>3</sub>. d) The intensity of  $\Delta T/T_0$  of *S*<sub>0</sub>, *S*<sub>1</sub>, *S*<sub>2</sub>, and *S*<sub>3</sub> at a time of 0 ps. e) TDOS of WSe<sub>2</sub> with atomic ratios (Se:W) of 2, 1.96, and 1.91666.

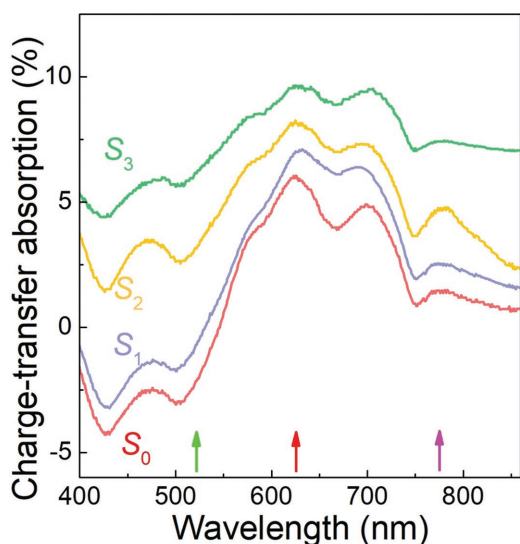


Figure 4. Charge-transfer absorption spectra of CuPc-WS<sub>2</sub> system.

peak originated from three samples is maintained at 629 nm, which is also increased from  $\approx 6$  a.u. on S<sub>0</sub> to  $\approx 9.6$  a.u. on S<sub>3</sub>. Moreover, the wavelengths of the excited laser are marked using arrows in Figure 4. Compared with 532 nm laser, the 632.8 and 706 nm laser beams are closer to the CT absorption

peak (629 nm) of three samples. The matching degree between excitation wavelength and the position of CT absorption peak will play an important role in charge-transfer resonance and the charge-transfer current. Generally, an increased matching degree between excitation wavelength and absorption position of sample will result in stronger charge-transfer current.

To quantitatively analyze the charge transfer at the interface of irradiated WS<sub>2</sub> and CuPc molecules, we detected the charge-transfer current using a hybrid BJT, where the charge-transfer current obtained as a weak signal is amplified.<sup>[37,38]</sup> Figure 5a shows the composite structure diagram of BJT. Graphene, CuPc, and WS<sub>2</sub> are sequentially stacked on the electrodes. At the contact of Au electrode and graphene, the surface potential profiles of graphene are bended, and the graphene transistor becomes an “n-p-n” channel<sup>[39]</sup> (Figure 5b). The stacked CuPc, WS<sub>2</sub>, and graphene constitute a photodiode (Figure 5c). Two electrodes and the graphene between electrodes were recognized as the emitter (E gate), collector (C gate), and base (B gate) in a standard BJT. Under the illumination, the photoinduced charge-transfer current ( $I_B$ ) generated at the interface of WS<sub>2</sub> and CuPc film was injected to B gate (Figure 5d). At a voltage ( $V_{CE}$ ) of 1 V,  $I_B$  is proportionally amplified to  $\Delta I = (I_{CE} - I_{CE0})$  as expressed by the following equation, where  $\beta$  is the amplification of BJT;  $I_{CE}$  and  $I_{CE0}$  are the current with or without light illumination;  $i$  is the wavelength of exciting laser (633–532 nm) (Supporting Information).

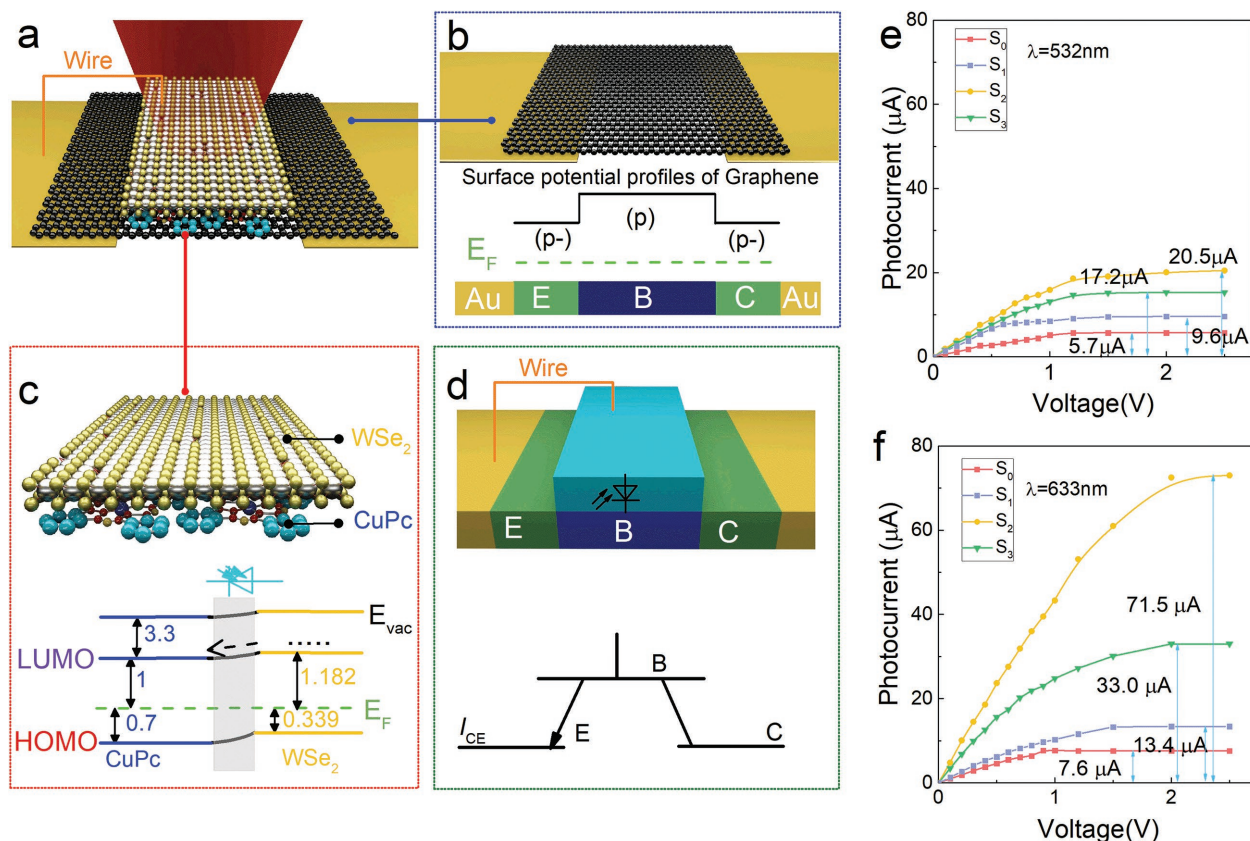


Figure 5. a) Composite structure diagram of BJT composed of WS<sub>2</sub>, CuPc, and graphene. b) Surface potential profiles of graphene on Au gates. c) Photodiode composed of stacked CuPc and WS<sub>2</sub>. d) Current model of bipolar diode. Evolution of amplified charge-transfer current excited by e) 532 nm laser and f) 632.8 nm laser.

$$\Delta I_i = I_{CE} - I_{CE0} = \beta I_B|_{V_{CE}=\text{const}} \quad (1)$$

Figure 5e shows the evolution of amplified charge-transfer current ( $\Delta I_{532}$ ) excited by a 532 nm laser.  $\Delta I_{532}$  slightly increased from 5.7 to 20.5  $\mu\text{A}$  with the decrease in atomic ratio from 2 ( $S_0$ ) to 1.96 ( $S_2$ ) and then dropped to 17.2  $\mu\text{A}$  at a ratio of 1.92 ( $S_3$ ). Figure 5f shows the charge-transfer current under an illumination of 632.8 nm laser.  $\Delta I_{633}$  is 71.5  $\mu\text{A}$  corresponding to the atomic ratio of 1.96 ( $S_2$ ), 9.4 times larger than  $S_0$  (7.6  $\mu\text{A}$ ). When the ratio was continuously decreased to 1.92,  $\Delta I_{633}$  decreased to 33.0  $\mu\text{A}$ . As the measured  $\Delta I$  is directly proportional to  $I_B$ , we can deduce the following: 1) The charge-transfer current excited by 632.8 nm laser is much more stronger than that excited by 532 nm laser. 2) The charge transfer on  $S_2$  is  $\approx 9.4$  times stronger than the as-prepared one. The current change in BJT should be related to the different charge-transfer level between CuPc and WSe<sub>2</sub>. Compared with 532 nm laser, the 632.8 nm laser is really closer to the resonance wavelength of CuPc, which has been verified by the absorption property in Figure 4. Based on the previous detection of exciton and charge transfer, the magnification mechanism of SERS shown in Figure 2 is discussed in detail.

## 2.4. SERS with Different Excitation Wavelengths

The 532 nm laser leads to a strong exciton resonance and a weak charge-transfer resonance; both the resonances are strong under the excitation of 632.8 nm laser. Hence, it can be concluded that the SERS under 532 nm laser is dominated by exciton resonance, and the SERS excited by 632.8 nm laser is the result of a joint effect of both the resonances. As shown in Figure 2b,e, both the low- and high-frequency vibrational modes in Raman spectroscopy are excited by the 632.8 nm laser, whereas the 532 nm laser only excites the high-frequency vibrational modes. More evidences are observed in the Raman spectra excited by 780 nm laser. On  $S_0$ ,  $S_1$ , and  $S_3$ , slight charge-transition absorption was observed at the excitation laser (Figure 4), and the intensity of Raman signal was concentrated on the high-frequency vibrational modes. However, on  $S_2$ , a new charge-transition absorption peak was observed at 780 nm, indicating the generation of a strong charge-transfer resonance. Because of this new charge-transfer resonance, the low-frequency vibrational modes from  $S_2$  (Figure 2f) showed a rapid increase and are almost three times as large as the high-frequency modes. This indicates that the charge-transfer resonance is dominant for the low-frequency modes of Raman signal.

## 2.5. Mechanism of Enhanced SERS Performance

According to the first-principle calculation and fs probe-pump measurement, the exciton resonance can be enhanced via decreasing the atomic ratio of WSe<sub>2</sub>, and the evolution of exciton resonance with atomic ratio is similar to the variation in the TDOS of WSe<sub>2</sub>. It seems that the decreased atomic ratio increases the TDOS of WSe<sub>2</sub>, providing more electronic states for photonic excitation. Besides, the intensity of exciton

increased by nine times on  $S_2$ , while the magnification of charge-transfer current is also 9.4 times on  $S_2$  with the same magnification. This is probably because of coupling of resonances, and the charge-transfer resonance borrows the energy from exciton resonance. In the molecule–semiconductor system, the charge-transfer resonance exists in three terms (known as A, B, and C terms). A-term is the resonance between the HOMO of molecule (valence band edge) to conduction band edge (LUMO of molecule). B-term originates from the molecule to semiconductor, and C-term is the opposite process of B-term. The relationship between the intensity of Raman signal ( $I$ ) and charge-transfer can be expressed by the following equation.<sup>[7]</sup>

$$I = [8\pi(\omega \pm \omega_{11})^4 I_L / 9C^4] \sum \alpha_{\sigma\rho}^2 \quad (2)$$

$$\alpha_{\sigma\rho} = A + B + C \quad (3)$$

where subscripts  $\sigma$  and  $\rho$  represent the components of polarizability tensor;  $I_L$  is the incident laser intensity at  $\omega$ ; and  $\omega_{11}$  is the molecular transition frequency between states  $I$  and  $I'$ ;  $\alpha$  is the polarizability. According to Equations (2) and (3), we can approximate that the SERS intensity is directly proportional to the square of charge transfer. In our measurement, the charge transfer increased by 9.4 times on  $S_2$  compared with the pristine WSe<sub>2</sub>. Hence, the SERS performance of  $S_2$  should be 88.4 times stronger than the pristine one. This speculation is almost twice of the measured results (more than 40 times) shown in Figure 2. It seems that there is still room for further exploitation of SERS performance by tailoring the atomic ratio of WSe<sub>2</sub>.

## 3. Conclusion

In this study, we demonstrate that the SERS performance of a WSe<sub>2</sub> monolayer can be adjusted by tailoring the atomic ratio of Se and W. The atomic ratio was tuned from 2 to 1.92 by ion irradiation. Based on the fs optical probe-pump measurement and charge-transfer current, it was found a reduced atomic ratio can increase the exciton and charge-transfer resonances in a CuPc–WSe<sub>2</sub> system, and the resonances can be correlated to the enhanced SERS performance. When excited by a 632.8 nm laser, the EF of CuPc film adsorbed onto the irradiated WSe<sub>2</sub> ( $R = 1.96$ ) is  $\approx 40$  times larger than the corresponding EF of the pristine film. Furthermore, the maximum EF on irradiated WSe<sub>2</sub> is more than 120. This study proposes a new avenue to tailor the SERS performance of 2D TMDCs and promote the application of TMDCs in SERS.

## 4. Experimental Section

**DFT Calculations:** The electron–ion interaction is described by the projector augmented wave (PAW) method. The energy cutoff of plane waves was set to 450 eV with an energy precision of  $10^{-5}$  eV. The electron exchange–correlation function was treated using a generalized gradient approximation (GGA) as proposed by Perdew, Burke, and Ernzerhof (PBE). The Monkhorst–Pack  $k$ -point meshes for the Brillouin zone (BZ) sampling used in structural optimization and electronic structure

calculations are  $3 \times 3 \times 1$  and  $5 \times 5 \times 1$ , respectively. A vacuum region of up to 15 Å was applied to exclude the interaction between adjacent images. Both the atomic positions were fully optimized using the conjugate gradient (CG) algorithm until the maximum atomic forces are less than  $0.001 \text{ eV \AA}^{-1}$ .

## Supporting Information

Supporting Information is available from the Wiley Online Library or from the author.

## Acknowledgements

The manuscript is written through contributions of all authors. All authors have given approval to the final version of the manuscript. Y.T. provided the origin idea, and is responsible for the organization and supervision of this work. This work was supported by the National Natural Science Foundation of China (Nos. 11535008, 11775136).

## Conflict of Interest

The authors declare no conflict of interest.

## Keywords

charge transfer, exciton, surface-enhanced Raman scattering, transition-metal dichalcogenides (TMDCs)

Received: August 16, 2018

Revised: September 16, 2018

Published online: October 31, 2018

- 
- [1] S. Nie, S. R. Emory, *Science* **1997**, 275, 1102.  
 [2] X. M. Lin, Y. Cui, Y. H. Xu, B. Ren, Z. Q. Tian, *Anal. Bioanal. Chem.* **2009**, 394, 1729.  
 [3] W. Ji, B. Zhao, Y. Ozaki, *J. Raman Spectrosc.* **2016**, 47, 51.  
 [4] G. C. Schatz, M. A. Young, R. P. Van Duyne, in *Surface-Enhanced Raman Scattering: Physics and Applications* (Eds: K. Kneipp, M. Moskovits, H. Kneipp), Springer, Berlin **2006**, p.19.  
 [5] G. C. Schatz, M. A. Young, R. P. Van Duyne, *Handbook of Vibrational Spectroscopy*, John Wiley and Sons, UK **2006**.  
 [6] J. J. Lin, L. B. Liang, X. Ling, S. Q. Zhang, N. N. Mao, N. Zhang, B. G. Sumpter, V. Meunier, L. M. Tong, J. Zhang, *J. Am. Chem. Soc.* **2015**, 137, 15511.  
 [7] J. R. Lombardi, R. L. Birke, *J. Phys. Chem. C* **2014**, 118, 11120.  
 [8] X. X. Han, W. Ji, B. Zhao, Y. Ozaki, *Nanoscale* **2017**, 9, 4847.  
 [9] P. S. Londero, M. Leona, J. R. Lombardi, *Appl. Phys. Lett.* **2013**, 102, 111101.  
 [10] X. X. Li, Y. Shang, J. Lin, A. R. Li, X. T. Wang, B. Li, L. Guo, *Adv. Funct. Mater.* **2018**, 28, 1801868.  
 [11] X. T. Wang, W. X. Shi, Z. Jin, W. F. Huang, J. Lin, G. H. Ma, S. Z. Li, L. Guo, *Angew. Chem., Int. Ed.* **2017**, 56, 9851.  
 [12] H. Li, Q. Zhang, C. C. R. Yap, B. K. Tay, T. H. T. Edwin, A. Olivier, D. Baillargeat, *Adv. Funct. Mater.* **2012**, 22, 1385.  
 [13] X. T. Wang, W. S. Shi, G. W. She, L. X. Mu, *J. Am. Chem. Soc.* **2011**, 133, 16518.  
 [14] J. Lin, Y. Shang, X. X. Li, J. Yu, X. T. Wang, L. Guo, *Adv. Mater.* **2017**, 29, 1604797.  
 [15] J. Lin, W. Hao, Y. Shang, X. T. Wang, D. L. Qiu, G. S. Ma, C. Chen, S. Z. Li, L. Guo, *Small* **2018**, 14, 1703274.  
 [16] L. B. Yang, D. Yin, Y. Shen, M. Yang, X. L. Li, X. X. Han, X. Jiang, B. Zhao, *Phys. Chem. Chem. Phys.* **2017**, 19, 18731.  
 [17] W. G. Xu, N. N. Mao, J. Zhang, *Small* **2013**, 9, 1206.  
 [18] C. Muehlethaler, C. R. Consideine, V. Menon, W. C. Lin, Y. H. Lee, J. R. Lombardi, *ACS Photonics* **2016**, 3, 1164.  
 [19] X. Ling, W. J. Fang, Y. H. Lee, P. T. Araujo, X. Zhang, J. F. Rodriguez-Nieva, Y. X. Lin, J. Zhang, J. Kong, *Nano Lett.* **2014**, 14, 3033.  
 [20] M. Samadi, N. Sarikhani, M. Zirak, H. Zhang, H. L. Zhang, A. Z. Moshfegh, *Nanoscale Horiz.* **2018**, 3, 90.  
 [21] Q. H. Wang, K. Kalantar-Zadeh, A. Kis, J. N. Coleman, M. S. Strano, *Nat. Nanotechnol.* **2012**, 7, 699.  
 [22] Y. Yin, P. Miao, Y. M. Zhang, J. C. Han, X. H. Zhang, Y. Gong, L. Gu, C. Y. Xu, T. Yao, P. Xu, Y. Wang, B. Song, S. Jin, *Adv. Funct. Mater.* **2017**, 27, 1606694.  
 [23] X. T. Wang, W. S. Shi, G. W. She, L. X. Mu, *Phys. Chem. Chem. Phys.* **2012**, 14, 5891.  
 [24] J. Lu, J. H. Lu, H. Liu, B. Liu, L. L. Gong, E. S. Tok, K. P. Loh, C. H. Sow, *Small* **2015**, 11, 1792.  
 [25] Z. H. Zheng, S. Cong, W. Gong, J. N. Xuan, G. H. Li, W. B. Lu, F. X. Geng, Z. G. Zhao, *Nat. Commun.* **2017**, 8, 1993.  
 [26] S. Cong, Y. Y. Yuan, Z. G. Chen, J. Y. Hou, M. Yang, Y. L. Su, Y. Y. Zhang, L. Li, Q. W. Li, F. X. Geng, Z. G. Zhao, *Nat. Commun.* **2015**, 6, 7800.  
 [27] X. Lian, Y. S. Wang, T. T. You, X. J. Zhang, N. Yang, G. S. Wang, P. G. Yin, *Nanoscale* **2017**, 9, 8879.  
 [28] H. Wang, H. Yuan, S. S. Hong, Y. Li, Y. Cui, *Chem. Soc. Rev.* **2015**, 44, 2664.  
 [29] P. Johari, V. B. Shenoy, *ACS Nano* **2012**, 6, 5449.  
 [30] D. Voiry, A. Goswami, R. Kappera, C. D. C. e Silva, D. Kaplan, T. Fujita, M. Chen, T. Asefa, M. Chhowalla, *Nat. Chem.* **2015**, 7, 45.  
 [31] Y. C. Lin, T. Björkman, H. P. Komsa, P. Y. Teng, C. H. Yeh, F. S. Huang, K. H. Lin, J. Jadcak, Y. S. Huang, P. W. Chiu, A. V. Krasheninnikov, *Nat. Commun.* **2015**, 6, 6736.  
 [32] Z. Lin, B. R. Carvalho, E. Kahn, R. T. Lv, R. H. Rao, H. Terrones, M. A. Pimenta, M. Terrones, *2D Mater.* **2016**, 3, 022002.  
 [33] Z. Q. Li, F. Chen, *Appl. Phys. Rev.* **2017**, 4, 011103.  
 [34] V. Vega-Mayoral, D. Vella, T. Borzda, I. Prijatelj, E. A. A. Pogna, S. D. Conte, P. Topolovsek, N. Vujicic, G. Cerullo, D. Mihailovic, C. Gadermaier, *Nanoscale* **2016**, 8, 5428.  
 [35] H. N. Wang, C. J. Zhang, F. Rana, *Nano Lett.* **2015**, 15, 339.  
 [36] H. B. Shu, Y. H. Li, X. H. Niu, J. L. Wang, *ACS Appl. Mater. Interfaces* **2016**, 8, 13150.  
 [37] Y. B. Lee, H. Kim, J. Lee, S. H. Yu, E. Hwang, C. Lee, J. H. Ahn, J. H. Cho, *Chem. Mater.* **2016**, 28, 180.  
 [38] P. Agnihotri, P. Dhakras, J. U. Lee, *Nano Lett.* **2016**, 16, 4355.  
 [39] F. Xia, T. Mueller, R. Golizadeh-Mojarad, M. Freitag, Y. Lin, J. Tsang, V. Perebeinos, P. Avouris, *Nano Lett.* **2009**, 9, 1039.